Journal of Sound and Vibration (1990) **142**(1), 49–75

NON-LINEAR DYNAMICS OF A SPUR GEAR PAIR

A. KAHRAMAN† AND R. SINGH

Department of Mechanical Engineering, The Ohio State University, 206 West 18th Avenue, Columbus, Ohio 43210, *U.S.A.*

(*Received* 6 *June* 1989, *and in final form* 27 *November* 1989)

Non-linear frequency response characteristics of a spur gear pair with backlash are examined in this paper for both external and internal excitations. The internal excitation is of importance from the high frequency noise and vibration control viewpoint and it represents the overall kinematic or static transmission error. Such problems may be significantly different from the rattle problems associated with external, low frequency torque excitation. Two solution methods, namely the digital simulation technique and the method of harmonic balance, have been used to develop the steady state solutions for the internal sinusoidal excitation. Difficulties associated with the determination of the multiple solutions at a given frequency in the digital simulation technique have been resolved, as one must search the entire initial conditions map. Such solutions and the transition frequencies for various impact situations are easily found by the method of harmonic balance. Further, the principle of superposition can be employed to analyze the periodic transmission error excitation and/or combined excitation problems provided that the excitation frequencies are sufficiently apart from each other. Our analytical predictions match satisfactorily with the limited experimental data available in the literature. Using the digital simulation, we have also observed that the chaotic and subharmonic resonances may exist in a gear pair depending upon the mean or design load, mean to alternating force ratio, damping and backlash. Specifically, the mean load determines the conditions for no impacts, single-sided impacts and double-sided impacts. Our results are different from the frequency response characteristics of the conventional, single-degree-of-freedom, clearance type non-linear system. Our formulation should form the basis of further analytical and experimental work in the geared rotor dynamics area.

1. INTRODUCTION

1.1. EXCITATION TYPES AND BACKLASH

The focus of this paper is on the backlash non-linearity as excited primarily by the transmission error between the spur gear pair. A gear pair is bound to have some backlash, which may be either designed to provide better lubrication and to eliminate interference or due to manufacturing errors and wear. Backlash-induced torsional vibrations may cause tooth separation and impacts in unloaded or lightly loaded geared drives. Such impacts result in intense vibration and noise problems and large dynamic loads, which may affect reliability and life of the gear drive [1, 2]. Excitation mechanisms can be grouped as follows.

(a) *External excitations.* This group includes excitations due to rotating mass unbalances, geometric eccentricities, and prime mover and/or load torque fluctuations [3]. Although mass unbalances and geometric eccentricities can be reduced through improved design and manufacturing, torque fluctuations are not easy to eliminate since they are determined by the characteristics of the prime mover (piston energies, d.c. motors etc.)

† Currently at General Motors Research Laboratories, Warren, Michigan 48090-9055, U.S.A.

0022-460X/90/190049+27/$03.00/0

and load [4]. Such excitations are typically at low frequencies $\bar{\Omega}_T$ which are the first few multiples of the input shaft speed $\bar{\Omega}_s$. Practical examples include rattle problems in lightly loaded automotive transmissions and machine tools [4, 5].

(b) *Internal excitations.* This group includes high frequency $\bar{\Omega}_h$ excitations caused by the manufacturing related profile and spacing errors, and the elastic deformation of teeth, shafts and bearings. Under the static conditions, all such mechanisms can be combined to yield an overall kinematic error function known as "the static transmission error" $\bar{e}(\bar{t})$ [2, 3]. This error is defined as the difference between the actual angular position of the driven gear and where it would be if the gears were perfect [2, 3, 6–8]. In gear dynamic models, $\bar{e}(\bar{t})$ is modelled as a periodic displacement excitation at the mesh point along the line of action [9–12] and its period is given by the fundamental meshing frequency $\bar{\Omega}_h = N\bar{\Omega}_s$, where N is the number of teeth on the pinion. Practical examples include steady state noise and vibration problems in automotive, aerospace, industrial, marine and appliance geared systems.

1.2. LITERATURE REVIEW

Experimental studies on the dynamic behavior of a spur gear pair with backlash started almost 30 years ago and still continue [13–15]. As one of the better examples of such experiments, Munro [13] developed a lightly damped (damping ratio $\zeta \approx 0{\cdot}02$) four-square test rig to measure the dynamic transmission error of a spur gear pair. He used high precision gears with rigid shafts and bearings, and showed experimentally that the tooth separation takes place when the mean load is less than the design load. Dynamic transmission error versus speed curves were plotted to illustrate the steady state response and the jump phenomenon. Kubo [14] measured the dynamic tooth stresses using a similar set-up in order to calculate the dynamic factors. He also observed a jump in the frequency response of the gear pair with backlash in spite of the test set-up being heavily damped ($\zeta \approx 0{\cdot}1$).

Such experimental studies, though limited in scope, have clearly shown that the gear pair dynamics cannot be predicted with a linear model—see the paper by Ozguven and Houser [16] for a detailed review of the linear gear dynamic models as available in the literature. Although most of the non-linear mathematical models used to describe the dynamic behavior of a gear pair are somewhat similar to each other, they differ in terms of the excitation mechanisms considered and the solution technique used. For instance, a large number of studies have been focused on the rattle problem in lightly loaded geared drives which are excited by the low frequency external torque excitations [17–22]. A few investigators have included the static transmission error excitation in the non-linear models [9, 22–24].

The gear backlash non-linearity is essentially a discontinuous and non-differentiable function and it represents a strong non-linear interaction in the governing differential equation. This issue has been discussed by Comparin and Singh [20] and they have concluded that most of the solution techniques available in the literature cannot be directly applied to examine this problem. Most of the gear dynamic researchers recognized this problem implicitly, and therefore employed either digital or analog simulation techniques [4, 9, 15, 19, 22–25]. For instance, Umezawa *et al.* [15], Yang and Lin [19] and Ozguven and Houser [9] have solved a one-degree-of-freedom torsional model of the gear pair using numerical techniques. Lin *et al.* [25] included motor and load inertias in a three-degree-of-freedom torsional model. Kucukay [22] has developed an eight-degree-of-freedom model to include the rocking and axial motions of the rigid shafts. In most of these studies, with the exception of Umezawa's analysis [15] which did not include any backlash, a discontinuity has been seen in the frequency response characteristics. But many investigators have typically joined two discrete points to show a broad jump in the

frequency response curve [9, 22, 25]. Some of these problems have been due to the numerical simulation techniques which may not work or may result in misleading answers if not employed properly. Such difficulties have been found by Comparin and Singh [20], Singh *et al.* [21] and Gear [26, 27], but are yet to be resolved or addressed by the gear dynamics researchers. Accordingly, one of the major objectives of this paper is to examine whether numerical simulation techniques can, in fact, be used to predict the dynamic response completely, and what precautions one must take to develop such a mathematical model. Since Comparin and Singh [20] and Singh *et al.* [21] have examined the external excitation problem, in this paper we focus mostly on the internal excitation and see whether the numerical simulation technique can be made to work for the prediction of the non-linear frequency response characteristics.

A few researchers have attempted to obtain the analytical solutions for a gear pair problem, based on the piece-wise linear techniques which divided the non-linear regime into several linear regimes [28–30]. For instance, Wang [28, 29] has used two- and three-degree-of-freedom torsional models with backlash, and assumed that the gear teeth are rigid and the driven gear has an infinite inertia. The governing equations have been solved by using the piece-wise linear technique. It should be noted, however, that the piece-wise linear technique gives only solutions for the equivalent linear systems and one typically may have difficulties in combining such solutions [30]. Comparin and Singh [20] overcame these problems by employing the harmonic balance method (HBM) and constructed analytical solutions for the non-linear frequency response characteristics of a gear pair with backlash as excited by the external torque. In this paper, we will use the same technique to examine the internal excitation problem, and compare results with digital simulation and experimental studies. Further literature review is included in subsequent sections.

2. PROBLEM FORMULATION

2.1. PHYSICAL MODEL

A two-degree-of-freedom semi-definite model of the spur gear pair with rotary inertias I_{g1} and I_{g2} and base circle diameters d_{g1} and d_{g2} as shown in Figure 1 is considered here (a list of symbols is given in the Appendix). The shafts and bearings are assumed to be rigid. The gear mesh is described by backlash of $2b$ and by a *time invariant mesh stiffness* $k_h \neq k_h(\bar{t})$ when in contact and viscous damping c_h. The equations of torsional motion

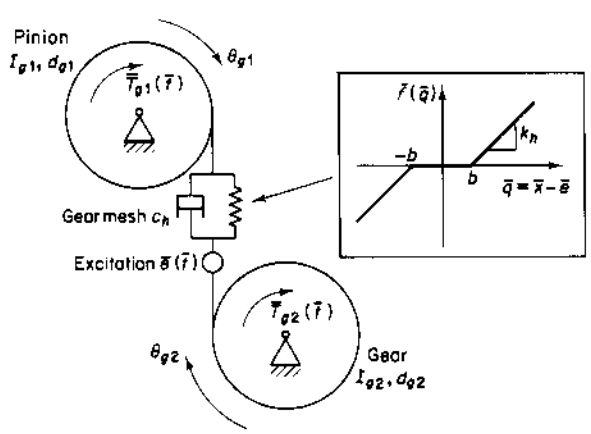

Figure 1. Gear pair model.

of the gear pair as shown in Figure 1 are

$$I_{g1}\frac{d^2\theta_{g1}}{d\bar{t}^2}+\frac{d_{g1}c_h}{2}\left(\frac{d_{g1}}{2}\frac{d\theta_{g1}}{d\bar{t}}-\frac{d_{g2}}{2}\frac{d\theta_{g2}}{d\bar{t}}-\frac{d\bar{e}}{d\bar{t}}\right)+\frac{d_{g1}}{2}\bar{f}\left(\frac{d_{g1}}{2}\theta_{g1}-\frac{d_{g2}}{2}\theta_{g2}-\bar{e}(\bar{t})\right)=\bar{T}_{g1}(\bar{t}), \quad (1a)$$

$$I_{g2}\frac{d^2\theta_{g2}}{d\bar{t}^2}-\frac{d_{g2}c_h}{2}\left(\frac{d_{g1}}{2}\frac{d\theta_{g1}}{d\bar{t}}-\frac{d_{g2}}{2}\frac{d\theta_{g2}}{d\bar{t}}-\frac{d\bar{e}}{d\bar{t}}\right)-\frac{d_{g2}}{2}\bar{f}\left(\frac{d_{g1}}{2}\theta_{g1}-\frac{d_{g2}}{2}\theta_{g2}-\bar{e}(\bar{t})\right)=-\bar{T}_{g2}(\bar{t}), \quad (1b)$$

where $\bar{T}_{g1}(\bar{t})=\bar{T}_{g1m}+\bar{T}_{g1a}(\bar{t})$ and $\bar{T}_{g2}(\bar{t})=\bar{T}_{g2m}+\bar{T}_{g2a}(\bar{t})$ are torques on pinion and gear and $\bar{f}$ is a non-analytical function essentially describing the mesh elastic force as shown in Figure 1. Here, output torque fluctuation $\bar{T}_{g2a}(\bar{t})$ will be neglected in order to simplify the dynamic problem: i.e., $\bar{T}_{g2}(\bar{t})=\bar{T}_{g2m}$. Equations (1a) and (1b) can be reduced to one equation in terms of $\bar{q}(\bar{t})$ which is defined as the difference between the dynamic transmission error $\bar{x}(\bar{t})$ and the static transmission error $\bar{e}(\bar{t})$: i.e.,

$$m_{c1}\frac{d^2\bar{q}}{d\bar{t}^2}+c_h\frac{d\bar{q}}{d\bar{t}}+k_h f(\bar{q}(\bar{t}))=\bar{F}_m+\bar{F}_{aT}(\bar{t})-m_{c1}\frac{d^2\bar{e}}{d\bar{t}^2}, \quad (2a)$$

$$\bar{q}(\bar{t})=\bar{x}(\bar{t})-\bar{e}(\bar{t})=(d_{g1}/2)\theta_{g1}(\bar{t})-(d_{g2}/2)\theta_{g2}(\bar{t})-\bar{e}(\bar{t}), \quad (2b)$$

$$m_{c1}=\frac{1}{\{(d_{g1}^2/4I_{g1})+(d_{g2}^2/4I_{g2})\}}, \qquad m_{c2}=4I_{g1}/d_{g1}, \quad (2c, d)$$

$$\bar{F}_m=2\bar{T}_{g1m}/d_{g1}=2\bar{T}_{g2m}/d_{g2}, \qquad \bar{F}_{aT}(\bar{t})=2m_c\bar{T}_{g1a}(\bar{t})/m_{c2}d_{g1}, \quad (2e, f)$$

$$f(\bar{q}(\bar{t}))=\frac{\bar{f}(\bar{q}(\bar{t}))}{k_h}=\begin{Bmatrix}\bar{q}(\bar{t})-b, & \bar{q}(\bar{t})>b\\ 0, & -b<\bar{q}(\bar{t})<b\\ \bar{q}(\bar{t})+b, & \bar{q}(\bar{t})<-b\end{Bmatrix}. \quad (2g)$$

Here m_{c1} is the equivalent gear pair mass, $\bar{F}_m$ is the average force transmitted through the gear pair, $\bar{F}_{aT}(\bar{t})$ is the fluctuating force related to the external input torque excitation and $f(\bar{q}(\bar{t}))$ is the non-linear displacement function. Equation (2a) is non-dimensionalized by letting $q(\bar{t})=\bar{q}(\bar{t})/b$, $\omega_n=\sqrt{k_h/m_{c1}}$, $t=\omega_n\bar{t}$ and $\zeta=c_h/(2m_{c1}\omega_n)$.

Now, consider harmonic excitation for both $\bar{e}(\bar{t})$ and $\bar{F}_{aT}(\bar{t})$ as $\bar{e}(\bar{t})=\tilde{e}\sin(\bar{\Omega}_h\bar{t}+\phi_h)$, $\bar{F}_{aT}(\bar{t})=\tilde{F}_{aT}\sin(\bar{\Omega}_T\bar{t}+\phi_T)$, where $\bar{\Omega}_h$ and $\bar{\Omega}_T$ are the fundamental excitation frequencies of internal displacement and external torque fluctuations, respectively. Further, define dimensionless excitation frequencies $\Omega_h=\bar{\Omega}_h/\omega_n$ and $\Omega_T=\bar{\Omega}_T/\omega_n$, dimensionless external mean load $F_m=\bar{F}_m/bk_h$, amplitudes of the dimensionless internal ($F_i(t)$) and external alternating forces ($F_e(t)$) $F_{aT}=\tilde{F}_{aT}/bk_h$ and $F_{ah}=\tilde{e}/b$ and the non-linear displacement function $f(q(t))$ to yield the following governing equation of motion:

$$\ddot{q}(t)+2\zeta\dot{q}(t)+f(q(t))=F(t), \quad (3a)$$

$$F(t)=F_m+F_{aT}\sin(\Omega_T t+\phi_T)+F_{ah}\Omega_h^2\sin(\Omega_h t+\phi_h), \quad (3b)$$

$$f(q(t))=\frac{f(\bar{q}(t))}{b}=\begin{Bmatrix}q(t)-1, & q(t)>1\\ 0, & -1<q(t)<1\\ q(t)+1, & q(t)<-1\end{Bmatrix}. \quad (3c)$$

2.2. SCOPE AND OBJECTIVES

When only external forces excite the system, i.e., $F_i(t)=0$, equation (3a) reduces to

$$\ddot{q}(t)+2\zeta\dot{q}(t)+f(q(t))=F_m+F_e(t)=F_m+F_{aT}\sin(\Omega_T t+\phi_T). \quad (4)$$

This equation has been solved both analytically and numerically by Comparin and Singh [20]. Conversely, no analytical solution is available when the system is excited by internal static transmission error at the mesh frequency Ω_h which is considerably higher than Ω_T. The governing equation is given by substituting $F_e(t) = 0$ in equation (3a) (note that the external mean load F_m is not equal to zero):

$$\ddot{q}(t) + 2\zeta\dot{q}(t) + f(q(t)) = F_m + F_i(t) = F_m + F_{ah}\Omega_h^2 \sin(\Omega_h t + \phi_h). \tag{5}$$

Both equations (4) and (5) include the clearance non-linearity. While equation (4) represents the conventional representation of the vibro-impact problem [20, 21], equation (5) is more applicable to the clearance problems in built-up assemblies where the excitation is generated by the kinematic errors. The proposed study is focused on the steady frequency response characteristics of equation (5) which represents a gear pair with backlash as excited harmonically by the static transmission error excitation $\bar{e}(\bar{t})$ or F_{ah}. Specific objectives are as follows.

1. Solve equation (5) numerically to resolve various modelling issues such as the existence of multiple solutions, subharmonic resonances and chaos.
2. Construct analytical solutions to equation (5) by using the harmonic balance method (HBM) which has been applied successfully to solve equation (4) by Comparin and Singh [20].
3. Compare digital simulation and harmonic balance techniques and establish the premises under which the jump phenomenon can be predicted.
4. Perform parametric studies in order to understand the effects of F_m, F_{ah} and ζ on the frequency response. Vary the force ratio $\hat{F} = F_m/F_{ah}$ which is a measure of the load on the gear pair and compare the dynamic behavior for lightly and heavily loaded gears.
5. Validate analytical and numerical solution techniques by comparing these with previous experimental studies [13, 14].
6. Compare the frequency response characteristics of equations (4) and (5), and also examine the possibility of finding overall response when both external and internal excitations are applied simultaneously.
7. Consider the periodic static transmission error excitation case, i.e.,

$$F(t) = F_m + F_i(t) = F_m + \sum_{j=1}^{k} (j\Omega_h)^2 F_{ahj} \sin(j\Omega_h t + \phi_{hj});$$

only the first three ($k = 3$) harmonics are included.

3. DIGITAL SIMULATION

Clearance or vibro-impact problems in single-degree-of-freedom systems have been examined by a number of investigators whose formulations are similar to equation (4)—see the paper by Comparin and Singh [20] for a detailed review. Moreover, Shaw and Holmes [30] and Moon and Shaw [31] have considered an elastic beam with one-sided amplitude constraint subject to a periodic displacement excitation, and have shown experimentally and numerically that the chaotic and subharmonic resonance regimes exist. Whiston [32–34] has investigated the non-linear response of a mechanical oscillator preloaded against a stop. He has solved the system equation for harmonic excitation by digital simulation and studied the existence and stability of the subharmonic and chaotic responses, and the effect of the preload on chaos. Similarly, Ueda [35] has solved the Duffing equation, $\ddot{q} + 2\zeta\dot{q} + q^3 = F \sin t$ numerically and defined the regions of different solutions on a ζ versus F map. According to him, the existence of harmonic, subharmonic

and chaotic responses depends on values of ζ and F, and multiple steady state solutions typically exist. Thompson and Stewart [36] have reviewed the available literature, with focus on Duffing's equation. It should be noted that equation (5) is different from the non-linear differential equations considered in the above-mentioned studies. Therefore, equation (5) must be studied in depth as the results of the other non-linear equations may not be directly applicable to our case.

First, we solve the governing non-linear differential equation (5) numerically using 5th–6th order, variable step Runge–Kutta numerical integration routine (DVERK of IMSL [37]) which is suitable for a strongly non-linear equation [20, 26, 27]. Second, we investigate the existence of chaos and subharmonic resonances. Since the steady state response of the system due to the sinusoidal excitation is of major interest, it is necessary to run the numerical program sufficiently long. The number of cycles of the forcing function required to reach the steady state depends on ζ.

A lightly loaded system ($\hat{F} = F_m/F_{ah} = 0{\cdot}5$) with low damping ($\zeta = 0{\cdot}02$) is considered as the first example case. For $F_m = 0{\cdot}1$ and $F_{ah} = 0{\cdot}2$, the response $q(t)$ is computed over the frequency range $0 < \Omega_h < 1{\cdot}5$. Phase plane plots $\dot{q}(t)$ *vs.* $q(t)$ for different Ω_h values are shown in Figure 2. For $\Omega_h = 0{\cdot}3$, all transients converge to one periodic solution at the fundamental frequency Ω_h of the forcing function irrespective of the initial conditions $q(0)$ and $\dot{q}(0)$. Therefore, it is called a "period-one, t_p" attractor, where $t_p = 2\pi/\Omega_h$. But, in the case of $\Omega_h = 0{\cdot}5$, three coexisting period-one attractors have been found as shown in Figure 2. Here, $q(0)$ and $\dot{q}(0)$ define three steady state limit cycle solutions. For all initial conditions given by $-2 < q(0) < 2$ and $-2 < \dot{q}(0) < 2$, a map of the domains of attraction for each steady state solution has been obtained and is shown in Figure 3. If a smaller increment is used for the initial conditions, a finer resolution will be obtained. Hence each phase plane plot shown in Figure 2 is strictly governed by a subset of the initial conditions. Similarly, two period-one attractors are found at $\Omega_h = 0{\cdot}6$. At $\Omega_h = 0{\cdot}7$, besides two period-one t_p attractors, two more solutions of period $3t_p$ exist: i.e., period-three attractors. But only a period-two $2t_p$ attractor is seen when $\Omega_h = 0{\cdot}8$. Within the range $1{\cdot}0 \leqslant \Omega_h \leqslant 1{\cdot}5$, non-periodic, steady state or chaotic response is observed. The chaotic time history and the Poincaré map (strange attractor) at $\Omega_h = 1{\cdot}0$ are shown in Figure 4. These results are qualitatively, but not quantitatively, similar to the studies reported on Duffing's equation [35, 36] and clearance non-linearity (equation (4) type) [20].

It is concluded that the subharmonic response of period nt_p provided that $n \neq 1$ and the chaotic response ($t_p \to \infty$) are seen in the gear pair only for a certain set of parameters F_m, $\hat{F}$, ζ and Ω_h. It must also be noted that the multi-solution regions are strongly dependent on the choice of $q(0)$ and $\dot{q}(0)$. Only one steady state solution can be found via digital simulation when only one set of initial conditions is chosen at a given Ω_h, and the rest of the steady state solutions are not predicted. This results in an incomplete frequency response description. These issues will be discussed further in section 5.

A heavily loaded system with $\hat{F} = 2$, $F_m = 0{\cdot}1$ and the same amount of damping $\zeta = 0{\cdot}02$ is considered as the second example case. In Figure 5 are shown the phase plane plots for the same values of Ω_h which are used in the first example case. Unlike the first example case, no chaotic responses are found here. All of the solutions are period-one t_p type for all $\Omega_h < 1{\cdot}0$, and the typical domains of attraction at $\Omega_h = 0{\cdot}6$ are shown in Figure 6. However, within the range $1{\cdot}0 \leqslant \Omega_h \leqslant 1{\cdot}5$, one period-two attractor coexists with the period-one orbit. Hence the force ratio $\hat{F}$ determines the existence of the chaotic and subharmonic responses. To illustrate this point, consider the chaos shown in Figure 4. As $\hat{F}$ and ζ are increased, significant changes in the response are observed in Figures 7 and 8. A transition from the chaos to a period-two, and then to a period-one steady state solution is seen when $\hat{F}$ is increased from 0·75 to 1·0 and then to 1·5. Similarly, an

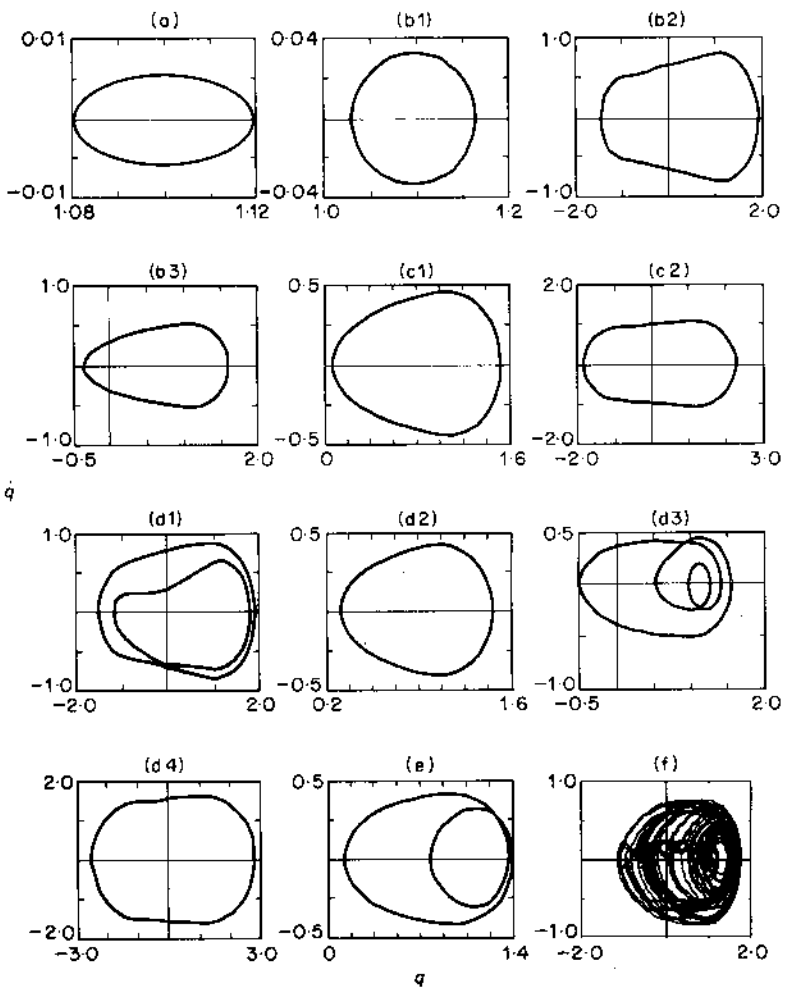

Figure 2. Phase plane plots of steady state solution $q(t)$ for $\hat{F} = 0{\cdot}5$, $F_m = 0{\cdot}1$, $\zeta = 0{\cdot}02$ and for different Ω_h values: (a) $\Omega_h = 0{\cdot}3$; (b) $\Omega_h = 0{\cdot}5$; (c) $\Omega_h = 0{\cdot}6$; (d) $\Omega_h = 0{\cdot}7$; (e) $\Omega_h = 0{\cdot}8$; (f) $\Omega_h = 1{\cdot}0$.

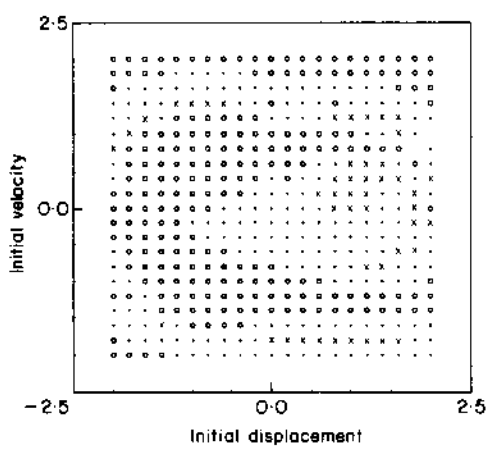

Figure 3. Domains of attraction for three attractors; ×, no impact (Figure 2(b1)); ·, single-sided impact (Figure 2(b3)), ○, double-sided impact (Figure 2(b2)); $\hat{F} = 0{\cdot}5$, $F_m = 0{\cdot}1$, $\zeta = 0{\cdot}02$ and $\Omega_h = 0{\cdot}5$.

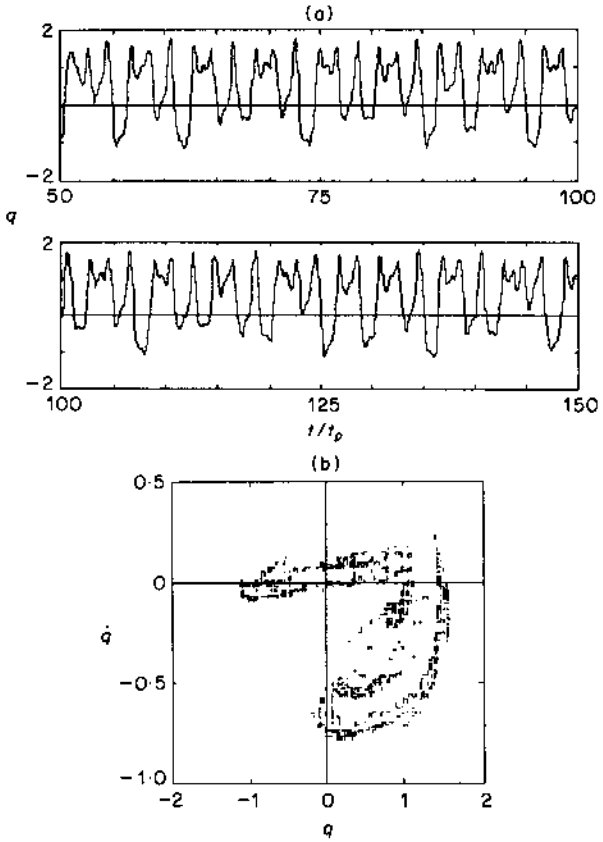

Figure 4. Chaotic response of a gear pair; $\hat{F} = 0{\cdot}5$, $F_m = 0{\cdot}1$, $\zeta = 0{\cdot}02$ and $\Omega_h = 1{\cdot}0$; (a) time history; (b) Poincaré map.

increase in ζ to 0·05 reduces chaos to a period-eight attractor, which then bifurcates to a period-two orbit at $\zeta = 0{\cdot}1$ as shown in Figure 8. Since most real geared systems are heavily loaded with a high $\hat{F}$, chaotic and subharmonic responses should not be seen under the normal driving conditions. This issue will be discussed again in section 6.

4. ANALYTICAL SOLUTION

An approximate solution for equation (5) can be constructed by using the harmonic balance method (HBM). Assume that $q(t) = q_m + q_a \sin(\Omega_h t + \phi_r)$, where q_m and q_a are mean and alternating components of the steady state response, and ϕ_r is the phase angle. Here, higher harmonics of the response are not included in the analysis. The quasi-linear approximation to the non-linear function $f(q)$ with the excitation $F(t) = F_m + F_i(t) = F_m + F_{ah}\Omega_h^2 \sin(\Omega_h t + \phi_h)$ is in the form [20, 38]

$$f(q) = N_m q_m + N_a q_a \sin(\Omega_h t + \phi_r) + N_a^* q_a \cos(\Omega_h t + \phi_r), \tag{6}$$

where the describing functions N_m, N_a and N_a^* are defined as

$$N_m = \frac{1}{2\pi q_m} \int_0^{2\pi} f(q_m + q_a \sin\varphi)\, \mathrm{d}\varphi, \tag{7a}$$

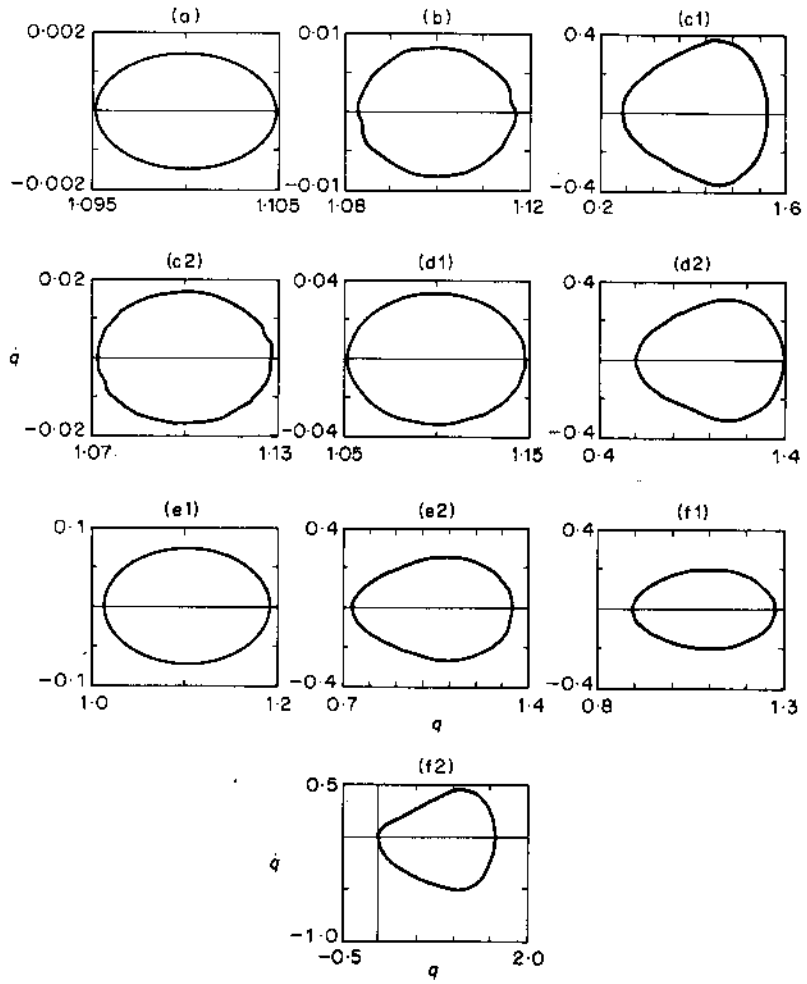

Figure 5. Phase plane plots of steady state solution $q(t)$ for $\hat{F}=2$, $F_m=0{\cdot}1$, $\zeta=0{\cdot}02$ and for different Ω_h values: (a) $\Omega_h=0{\cdot}3$; (b) $\Omega_h=0{\cdot}5$; (c) $\Omega_h=0{\cdot}6$; (d) $\Omega_h=0{\cdot}7$; (e) $\Omega_h=0{\cdot}8$; (f) $\Omega_h=1{\cdot}0$.

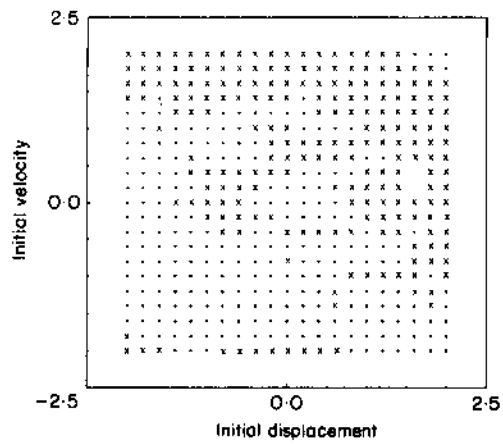

Figure 6. Domains of attraction for two attractors; ×, no impact (Figure 5(c2)); ·, single sided impact (Figure 5(c1)); $\hat{F}=2$, $F_m=0{\cdot}1$, $\zeta=0{\cdot}02$ and $\Omega_h=0{\cdot}6$.

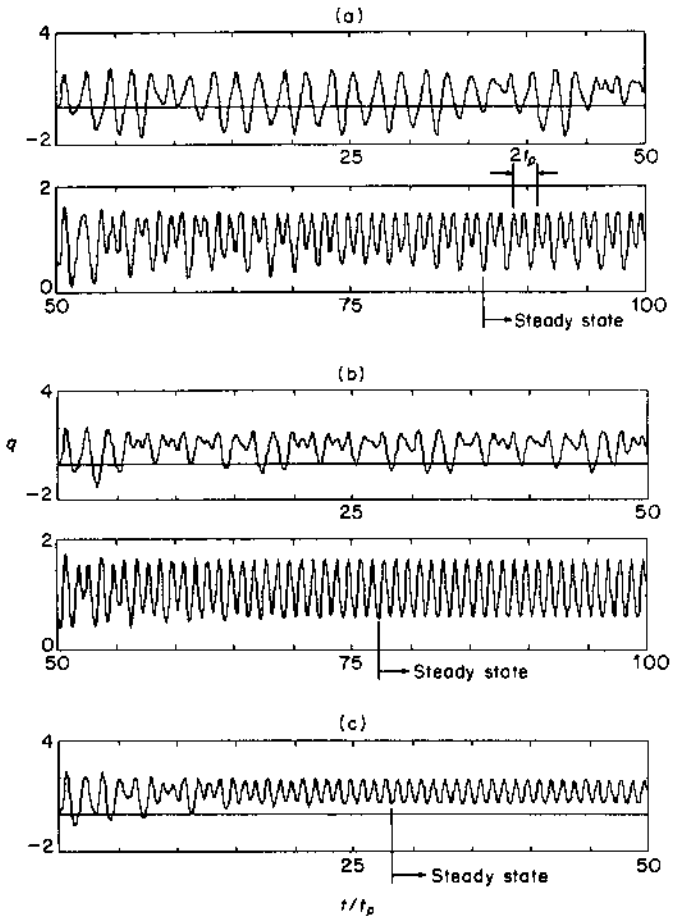

Figure 7. Time histories of $q(t)$ for $F_{ah} = 0{\cdot}2$, $\zeta = 0{\cdot}02$ and (a) $\hat{F} = 0{\cdot}75$, (b) $\hat{F} = 1$, (c) $\hat{F} = 1{\cdot}5$.

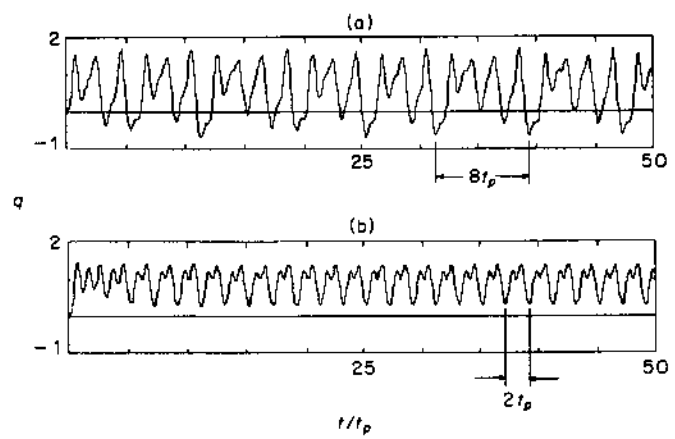

Figure 8. Time histories of $q(t)$ for $F_m = 0{\cdot}1$, $\hat{F} = 0{\cdot}5$ and (a) $\zeta = 0{\cdot}05$, (b) $\zeta = 0{\cdot}1$.

$$N_a = \frac{1}{\pi q_a}\int_0^{2\pi} f(q_m + q_a \sin\varphi)\sin\varphi \, d\varphi, \tag{7b}$$

$$N_a^* = \frac{1}{\pi q_a}\int_0^{2\pi} f(q_m + q_a \sin\varphi)\cos\varphi \, d\varphi, \qquad \varphi = \Omega_h t + \phi_r. \tag{7c, d}$$

Equation (3b) is substituted into equations (7a), (7b) and (7c) to obtain

$$N_m = 1 - (q_a/2q_m)[g(\gamma_+) - g(\gamma_-)], \qquad N_a = 1 - \tfrac{1}{2}[h(\gamma_+) + h(\gamma_-)], \tag{8a, b}$$

$$N_a^* = 0, \qquad \gamma_\pm = (1 \pm q_m)/q_a \tag{8c, d}$$

where

$$g(\gamma) = \begin{cases} (2/\pi)(\gamma \sin^{-1}\gamma + \sqrt{1-\gamma^2}), & |\gamma| \le 1 \\ |\gamma|, & |\gamma| > 1 \end{cases}, \tag{8e}$$

$$h(\gamma) = \begin{cases} (2/\pi)(\sin^{-1}\gamma + \gamma\sqrt{1-\gamma^2}), & |\gamma| \le 1 \\ -1, & \gamma < -1 \\ 1, & \gamma > 1 \end{cases}. \tag{8f}$$

Comparin and Singh [20] used truncated series expansions for the functions $g(\gamma)$ and $h(\gamma)$ given by equations (8e) and (8f). They stated that the error involved in using truncated series is within 6% when only the first two terms are considered with the coefficient of the second term adjusted to yield the actual value for $\gamma = 1$. Using the same approach, one gets

$$g(\gamma) \cong \frac{2}{\pi}\left(1 + \left(\frac{\pi - 2}{\pi}\right)\gamma^2\right), \quad h(\gamma) \cong \frac{4}{\pi}\left(\gamma - \left(\frac{4-\pi}{4}\right)\gamma^3\right), \qquad |\gamma| \le 1, \tag{9a, b}$$

and obtains the following frequency response by substituting equations (4) and (5) into equation (3a) and equalizing the coefficients of like harmonics:

$$q_a = \frac{F_{ah}\Omega_h^2}{\sqrt{(N_a - \Omega_h^2)^2 + (2\zeta\Omega_h)^2}}, \qquad q_m = \frac{F_m}{N_m}, \qquad \phi_r = \phi_h - \tan^{-1}\left\{\frac{2\zeta\Omega_h}{N_a - \Omega_h^2}\right\}. \tag{10a, b, c}$$

Depending on the damping ratio ζ and the parameters F_m, F_{ah} and Ω_h which define the excitation, there are three cases at which different solutions are obtained: (a) no impact (no tooth separation); (b) single-sided impacts (tooth separation, but no back collision); (c) two-sided impacts (back collision).

Case I: no impact. The tooth separation (impact) is not observed in a geared system if the displacement $q(t)$ lies in the region $q(t) > 1$ all the time. This condition, shown in Figure 9 as case I, can be described mathematically as

$$|q_m + q_a| > 1 \qquad \text{and} \qquad |q_m - q_a| > 1. \tag{11}$$

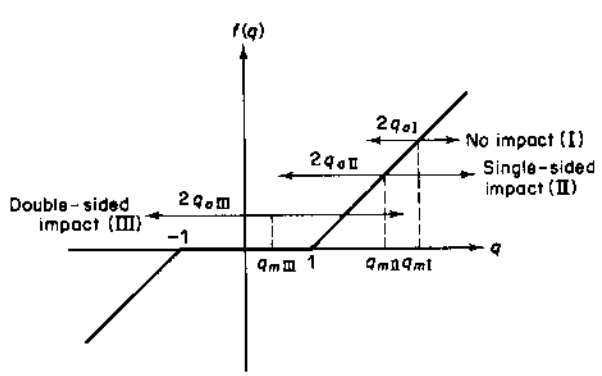

Figure 9. Illustration of different impact regimes.

Then, for no impact region in which the conditions defined by equation (11) are satisfied, the describing functions are given by

$$N_m = 1 - 1/q_m, \qquad N_a = 1. \tag{12a, b}$$

Substitution of equations (12) into equations (9) yields the following governing equations for no-impact case

$$q_{aI} = \frac{F_{ah}\Omega_h^2}{\sqrt{(1-\Omega_h^2)^2 + (2\zeta\Omega_h)^2}}, \qquad q_{mI} = F_m + 1, \qquad \phi_{hI} = \phi_p - \tan^{-1}\left(\frac{2\zeta\Omega_h}{1-\Omega_h^2}\right). \tag{13a, b, c}$$

Hence, when there is no tooth separation, the system is linear and mean and alternating components of the response, q_m and q_a, are uncoupled from each other. The transition frequencies from no-impact (linear) regime to the other non-linear regimes where tooth separation occurs are found by substituting $q_a = |q_m - 1|$ into the equations (13a) and (13c) as

$$\Omega_{t2,t1} = \sqrt{\frac{(1-2\zeta^2) \pm \sqrt{(1-2\zeta^2)^2 - \{1-(F_{ah}/F_m)^2\}}}{\{1-(F_{ah}/F_m)^2\}}}, \tag{14}$$

where Ω_{t1} and Ω_{t2} are the transition frequencies from no impact to single-sided impact regimes below and above resonance, respectively.

Case II: single-sided impact. Mathematically, the single-sided impacts (tooth separation without back collision) are observed if

$$q_m + q_a > 1 \qquad \text{and} \qquad |q_m - q_a| < 1. \tag{15}$$

As illustrated in Figure 9 as case II, the solution remains in the region $q(t) > -1$. The describing functions satisfying equation (15) are of the form

$$N_m = 1 - (q_{aII}/2q_{mII})[\gamma_+ - g(\gamma_-)], \qquad N_a = 1 - \tfrac{1}{2}[1 + h(\gamma_-)]. \tag{16a, b}$$

Substitution of equations (10a) and (10b) into equations (16a) and (16b) gives the describing functions for the single-sided impact case:

$$N_m = 1 + \frac{q_{aII}}{2q_{mII}}\left\{\frac{2}{\pi}\left[1 + \left(\frac{\pi-2}{2}\right)(\gamma_-)^2\right] - (\gamma_+)\right\}, \tag{17a}$$

$$N_a = \frac{1}{2} - \frac{2(1-q_{mII})}{\pi q_{aII}}\left[1 - \left(\frac{4-\pi}{4}\right)(\gamma_-)^2\right]. \tag{17b}$$

Then equations (9a), (9b) and (9c) with the describing functions given by equations (17a) and (17b) define the response of the system in the single-sided impact region. In this case, it is hard to find closed form expressions for transition frequencies from single-sided to double-sided impact regions. The validity of the solutions, obtained by solving equations (9) and (17) iteratively, should be checked. If the solution does not satisfy the equation (15), then single sided impacts are not seen at that particular frequency.

Case III: double-sided impact. Double-sided impact case exists if q_m and q_a are such that the following conditions are satisfied:

$$q_a > |1 - q_m| \qquad \text{and} \qquad q_a > |1 + q_m|. \tag{18}$$

Figure 9 (case III) shows the double-sided impact case at which q_a is large enough when compared to q_m so that back collision is observed. The describing functions for this case are obtained from equations (8a) and (8b) under the condition given by equations (19):

$$N_m = 1 - \frac{2(\pi-2)}{\pi q_{aIII}}, \qquad N_a = 1 - \frac{4}{\pi}\left[\frac{1}{q_{aIII}} - \left(\frac{4-\pi}{4}\right)\left(\frac{1+3q_{mIII}^2}{q_{aIII}^3}\right)\right]. \tag{19a, b}$$

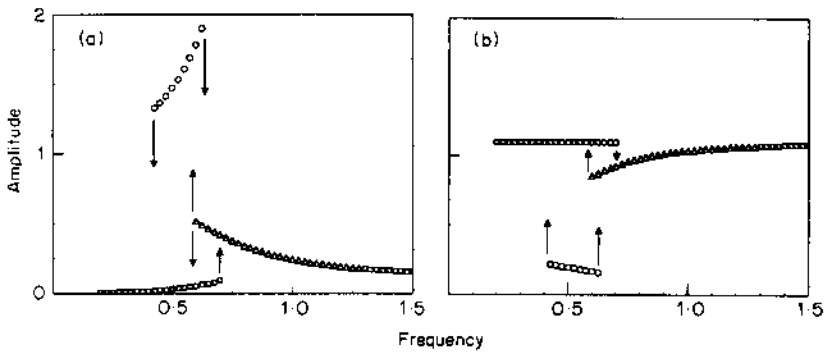

Figure 10. Typical frequency response plots for a gear pair; (a) q_a versus Ω_h; (b) q_m versus Ω_h. □, Case I; △, case II; ○, case III.

The solution for the double-sided impact case is obtained by solving equations (9) and (19) numerically. The validity of the solution, again, should be examined by using the conditions defined by equation (18), as it is done in the single-sided impact case.

The solutions of all three regimes are combined to obtain the overall frequency response of the gear pair. Typical q_a versus Ω_h and q_m versus Ω_h plots are illustrated in Figure 10. All three impact regimes are shown on these plots. Also we note the frequency region where multiple steady state solutions are obtained.

5. COMPARISON OF TWO SOLUTION METHODS

First, we validate the approximate analytical solutions of equation (5) by comparing predictions with the results obtained by digital simulation. Again, two example cases (a heavily loaded system and a lightly loaded system) are considered and the frequency response curves q_a versus Ω_h and q_m versus Ω_h are generated. In Figure 11 is shown the frequency response for the heavily loaded system with $\hat{F} = 2$, $F_m = 0{\cdot}1$ and $\zeta = 0{\cdot}05$. Numerical and analytical results agree very well as both predict amplitudes and the transition frequencies for case I (no impact) and case II (single-sided impact) regimes, and both show that the double-sided impact solutions do not exist. These results demonstrate that the analytical solutions are indeed correct for the heavily loaded system. Now consider the lightly loaded system as the second example case with $\hat{F} = 0{\cdot}5$, $F_m = 0{\cdot}1$ and $\zeta = 0{\cdot}05$. From Figure 12 we note that while case I and case II solutions as yielded by

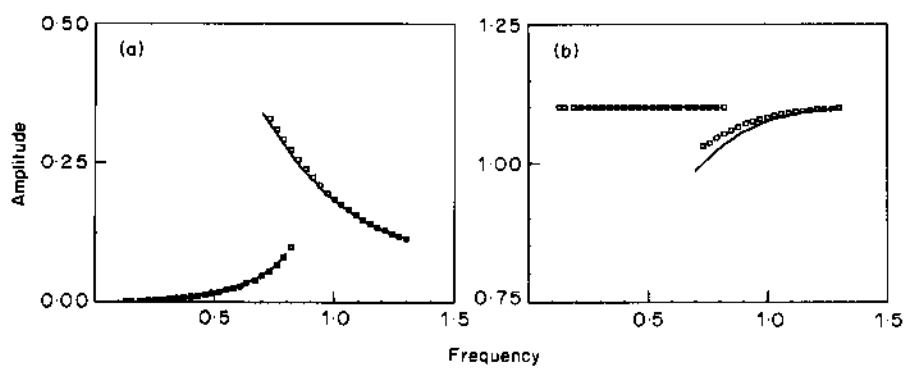

Figure 11. Comparison of theory (——) with numerical simulation (□); $F_m = 0{\cdot}1$, $\hat{F} = 2$, $\zeta = 0{\cdot}05$; (a) q_a versus Ω_h; (b) q_m versus Ω_h.

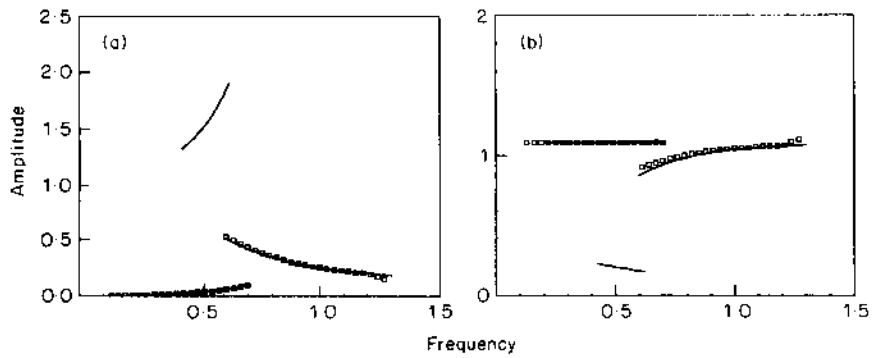

Figure 12. Comparison of theory with numerical simulation; $F_m = 0{\cdot}1$, $\hat{F} = 0{\cdot}5$, $\zeta = 0{\cdot}05$; (a) q_u versus Ω_h; (b) q_m versus Ω_h. Key as Figure 11.

both solution techniques are very close to each other, case III regime is predicted only by the analytical expressions. Why is case III not predicted by the digital simulation? To answer this consider the following.

(a) In digital simulation, several sets of $q(0)$ and $\dot{q}(0)$ must be tried to find all of the steady state solutions within a multi-valued region, for instance $0{\cdot}6 \leqslant \Omega_h \leqslant 0{\cdot}7$ in Figure 11 and $0{\cdot}4 \leqslant \Omega_h \leqslant 0{\cdot}7$ in Figure 12. When $q(0)$ and $\dot{q}(0)$ are kept constant for each Ω_h or if the steady state solution of the previous frequency is used as the basis for the initial conditions for the next frequency considered, only one of the solutions can be found while missing the other(s). Figure 13 illustrates this point, as the steady state solution of the previous frequency is used here for the initial conditions at each Ω_h. With this procedure, case II solutions within the multi-valued regions are missed. Therefore, whenever digital simulation is used to solve the equation of motion, dependence of the steady state solutions on $q(0)$ and $\dot{q}(0)$ must be taken into account to avoid the risk of obtaining an incomplete frequency response description as obtained by a few previous investigators [9, 25].

(b) In the case of Figure 12, no initial conditions governed by case III are found by the digital simulation within the range of initial conditions $-2 < q(0) < 2$ and $-2 < \dot{q}(0) < 2$ we have considered. Conversely, the analytical method predicts this regime as the issue of initial conditions is irrelevant here. To illustrate this, first we consider the case of Figure 3 with $\hat{F} = 0{\cdot}5$, $F_m = 0{\cdot}1$, $\zeta = 0{\cdot}02$ and $\Omega_h = 0{\cdot}5$. In Figure 14(a) is shown the domain of attraction governed by case III within the range $-2 < q(0) < 2$ and $-2 < \dot{q}(0) < 2$

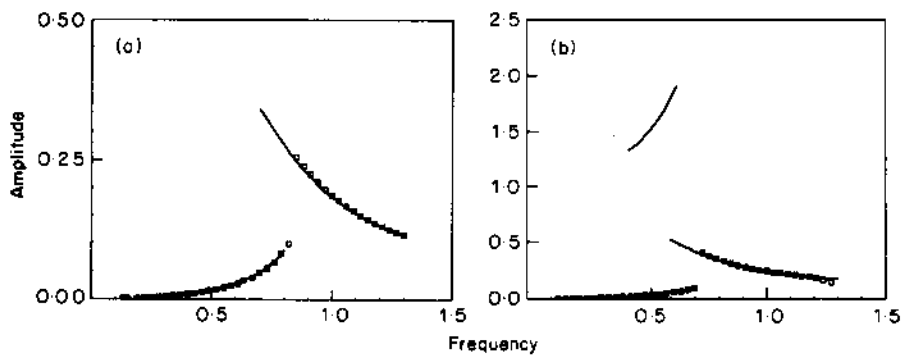

Figure 13. Comparison of theory with numerical simulation when initial conditions are kept constant; $F_m = 0{\cdot}1$, $\zeta = 0{\cdot}05$; (a) $\hat{F} = 2$; (b) $\hat{F} = 0{\cdot}5$. Key as Figure 11.

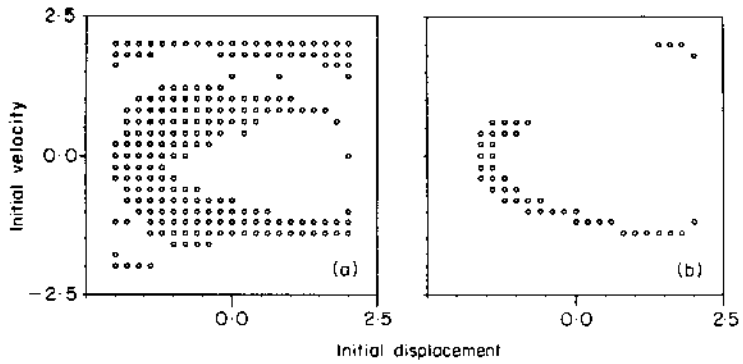

Figure 14. Domains of attraction for case III solutions for $F_m = 0{\cdot}1$, $\hat{F} = 0{\cdot}5$, $\Omega_h = 0{\cdot}5$; (a) $\zeta = 0{\cdot}02$; (b) $\zeta = 0{\cdot}03$.

with a $q(0)$ or $\dot{q}(0)$ increment of 0·2. Here, almost half of the initial conditions considered define case III solutions. Therefore the chance of having a double sided impact solution at $\Omega_h = 0{\cdot}5$ is considerably high. Now, increase the damping to $\zeta = 0{\cdot}03$. Once again a case III regime is predicted analytically, but the number of initial conditions corresponding to case III is not sufficiently high, like the case of $\zeta = 0{\cdot}02$. In the digital simulation, the transient solution will converge to the case I or case II solution unless the initial condition corresponds to one of those shown in Figure 14(b) for case III. The limiting case is reached when $\zeta = 0{\cdot}04$, while holding the other parameters the same; now no initial conditions corresponding to case III are found. Obviously there might be initial conditions, out of the range considered, which correspond to the analytical results. Therefore the existence of case III solutions should be checked numerically by searching the entire range of initial conditions as defined by the physical considerations of the system.

6. PARAMETRIC STUDIES

Frequency response amplitudes, transition frequencies and the existence of various impact regimes depend on F_m, $\hat{F}$ and ζ. Therefore, a set of parametric studies in which the analytical solutions of section 4 were used will be presented here; the same results can be duplicated by the digital simulation technique. First we examine the effect of F_m and $\hat{F}$ while holding the damping ratio ζ equal to 0·05. Results for four different $\hat{F}$ values obtained by varying F_{ah} for a given $F_m = 0{\cdot}1$ are compared in Figures 15 and 16. Both gears maintain complete contact with each other when $\hat{F}$ is very large, say $\hat{F} = 10$ in Figures 15(a) and 16(a). Consequently the dynamic system is linear and the mean q_m and alternating q_a components of the torsional motion are uncoupled as expected. However, for $\hat{F} = 2$, the no-impact regime (case I) cannot cover the whole frequency range and a region around the resonant frequency is dictated by the single-sided impacts (case II). Away from the resonance, over the range given by $\Omega_h > 0{\cdot}8$ and $\Omega_h < 0{\cdot}7$, solutions are single-valued whether one has case I or case II solutions. Conversely, near the resonance given by $0{\cdot}7 < \Omega_h < 0{\cdot}8$ dual-valued solutions are seen in Figures 15(b) and 16(b). Also sudden discontinuities are observed: i.e., a jump up at $\Omega_h = 0{\cdot}8$ and a jump down at $\Omega_h = 0{\cdot}7$. When $\hat{F}$ is reduced further, double-sided impact (case III) solutions start to appear in Figures 15(c) and 16(c). Now the frequency range of interest can be divided into the following four regions: (i) case I, $\Omega_h < 0{\cdot}4$; (ii) case I and case III, $0{\cdot}4 < \Omega_h < 0{\cdot}6$; (iii) all three cases, $0{\cdot}6 < \Omega_h < 0{\cdot}625$; (iv) only case II, $\Omega_h > 0{\cdot}625$. Region (ii) disappears at $\hat{F} > 0{\cdot}5$.

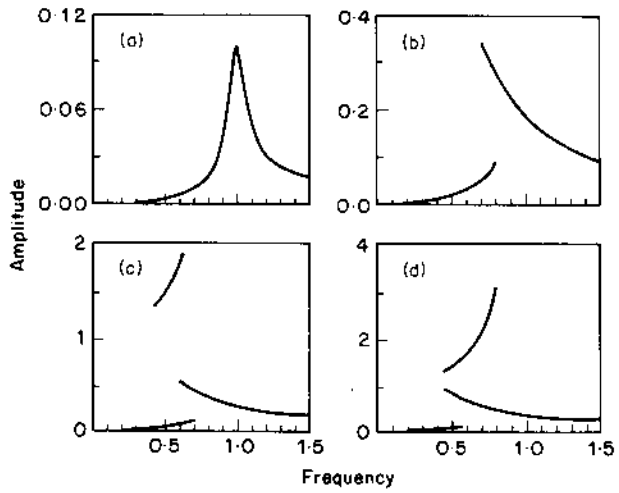

Figure 15. Frequency response q_a for different alternating loads; $F_m = 0{\cdot}1$, $\zeta = 0{\cdot}05$; (a) $\hat{F} = 10$; (b) $\hat{F} = 2$; (c) $\hat{F} = 1$; (d) $\hat{F} = 0{\cdot}5$.

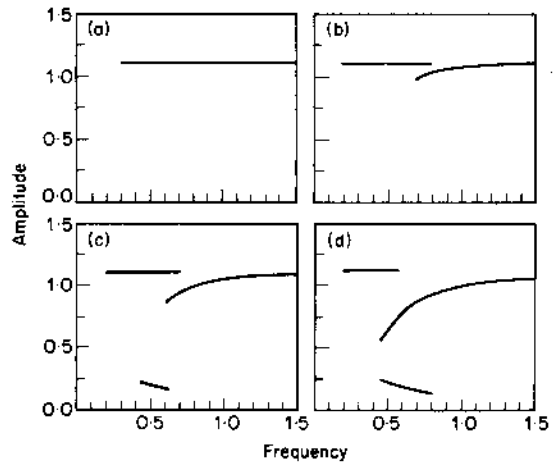

Figure 16. Frequency response q_m for different alternating loads; $F_m = 0{\cdot}1$, $\zeta = 0{\cdot}05$; (a) $\hat{F} = 10$; (b) $\hat{F} = 2$; (c) $\hat{F} = 1$; (d) $\hat{F} = 0{\cdot}5$.

Next, we vary $\hat{F}$ by changing F_m for a given $F_{ah} = 0{\cdot}05$. This set of parameters does not yield any double-sided impacts (case III). Again, the tooth pair does not lose contact when $\hat{F}$ is large enough, say $\hat{F} \geqslant 10$ and only the linear solutions exist, as shown in Figure 17(a). But when $\hat{F}$ is lowered to $\hat{F} = 4, 2$ and 1, the response is non-linear, which is composed of cases I and II as shown in Figures 17(b)–(d).

Next we examine the role of damping ratio ζ on the frequency response in Figure 18, given $F_m = 0{\cdot}1$ and $F_{ah} = 2$. Double-sided impacts are found at a low damping value $\zeta = 0{\cdot}025$ as shown in Figure 18(a). When ζ is increased to 0·05, case III solutions no longer exist and case I and case II solutions define the frequency response completely. The jump-up and jump-down transition frequencies in Figure 18(b) are distinctly apart. With an increase in ζ, transition frequencies approach each other which narrows the dual-valued solution region. At $\zeta = 0{\cdot}1$, the frequency response is single valued and the jump-up and jump-down transitions in Figure 18(d) take place almost at the same

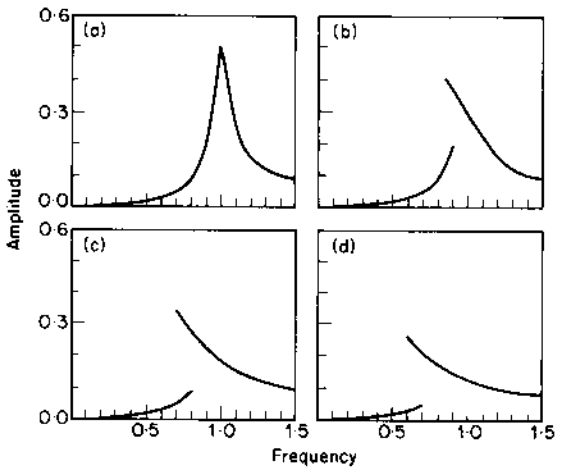

Figure 17. Frequency response q_a for different mean loads; $F_{ah} = 0{\cdot}05$, $\zeta = 0{\cdot}05$; (a) $\hat{F} = 10$; (b) $\hat{F} = 4$; (c) $\hat{F} = 2$; (d) $\hat{F} = 1$.

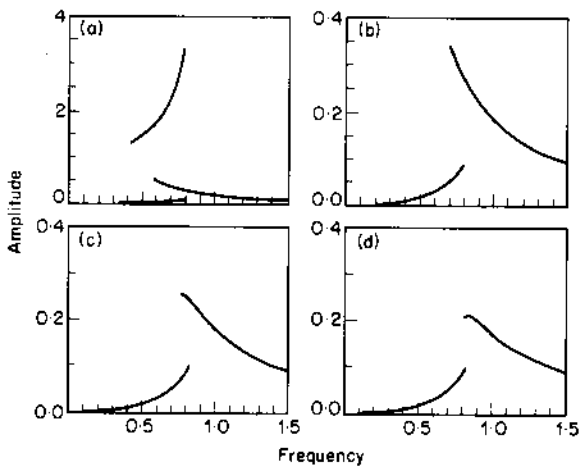

Figure 18. Frequency response q_a for different damping values; $F_m = 0{\cdot}1$, $\hat{F} = 2$, and (a) $\zeta = 0{\cdot}025$, (b) $\zeta = 0{\cdot}05$, (c) $\zeta = 0{\cdot}075$, (d) $\zeta = 0{\cdot}1$.

frequency. Finally, as for the linear systems, the damping ratio also lowers the amplitudes in the non-linear resonance regime.

7. EXPERIMENTAL VALIDATION

Our analytical solutions of section 4 will be compared with the experimental results of Munro [13], who used a four-square test rig to measure the dynamic transmission error $\bar{x}(\bar{t})$ of a spur gear pair. High precision spur gears with manufacturing errors much smaller than tooth deflections were selected. Pinion and gear were identical with 32 teeth, face width of 12·7 mm and diametral pitch of 4. Tooth profile modifications were applied to obtain a minimum (but not zero) $\bar{e}(\bar{t})$ at the design load of 3780 N. Other components of the set-up including shafts, bearings and casing were made as rigid as possible in order to simulate the configuration shown in Figure 1. $\bar{x}(\bar{t})$ was measured for a range of gear mesh excitation frequencies under different mean loads $\bar{F}_m$. Some of the key parameters

were not specified by Munro [13]. For example, it was stated that some additional inertias were added to the gears to shift the primary resonant frequency within the operational speed range, but the specific values of such inertias were not given. It was also reported that the damping ratio ζ varies with load "in a random manner". Also, backlash was not measured or reported. Therefore, in our study, we estimate the damping ratio ($\zeta = 0{\cdot}0175$) and the resonant frequency ω_n by considering the design load case at which only linear behavior is seen; time-invariant mesh stiffness is assumed in the model. The same value of ζ is used at each discrete load $\bar{F}_m$ and a backlash value of $2b = 0{\cdot}1$ mm is assumed in our model.

The measured and predicted frequency response of the dynamic transmission error $\bar{x}(\bar{t})$, on a peak to peak basis, at the design load and at 1/4, 1/2 and 3/4 of the design load, respectively are compared in Figure 19-22. As shown in Figure 19, both analytical and experimental results indicate that teeth maintain contact at the design load and hence the system behaves as a linear system in spite of the backlash. This is because the static transmission error $\bar{e}(\bar{t})$ is minimum at the design load which results in a large force ratio F_m/F_a, say 50. However, when the mean load $\bar{F}_m$ is lowered to $\frac{3}{4}$ of the design load which corresponds to a larger static transmission error $\bar{e}(\bar{t})$, tooth separation takes place. Consequently we note a jump in the frequency response as shown in Figure 20 for both

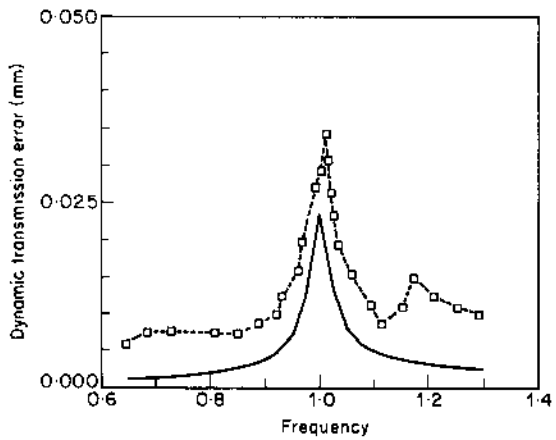

Figure 19. Comparison of the theory (——) with Munro's [13] experiments (- - □ - -) at design load.

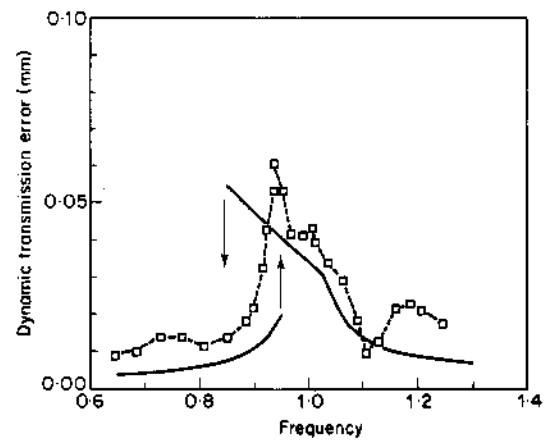

Figure 20. Comparison of theory with Munro's [13] experiments at 3/4 of design load. Key as Figure 19.

analysis and experiment. This jump phenomenon is more noticeable at $\frac{1}{2}$ and $\frac{1}{4}$ of the design loads as shown in Figures 21 and 22, respectively. Our theory matches very well with Munro's experimental results [13] in spite of the lack of knowledge of some relevant parameters.

As the second example case, the experimental results of Kubo [14] are considered and compared with our theory. Experimental results and the relevant system parameters are extracted from a recent paper by Ozguven and Houser [9], and the excitation $\bar{e}(\bar{t})$ is calculated for a spur gear elastic model [6]. Kubo designed a four-square spur gear test rig which was heavily damped ($\zeta \approx 0{\cdot}1$). He measured dynamic root stresses σ_d and then estimated the dynamic factor D_S as $D_S = \sigma_d/\sigma_s$, where σ_s is the static tooth root stress. However, in several other studies [1] the dynamic factor is defined as the ratio of the dynamic mesh load $\bar{F}_d$ to static mesh load $\bar{F}_m$, given by $D_L = \bar{F}_d/\bar{F}_m = F_d/F_m = \{2\zeta\dot{q}(t) + f(q(t))\}/F_m$. Note that D_L is equal to D_S when the change of the moment arm due to a change in contact point is neglected. In Figure 23 is shown the envelope of dynamic factor D_S, measured for eight different teeth pairs, and the D_L spectrum computed by using the analytical solutions of section 4. Here, at most of the frequencies, our predictions are not within the measured envelope, but the transition frequency and the amplitude at the jump discontinuity are predicted accurately. There might be several

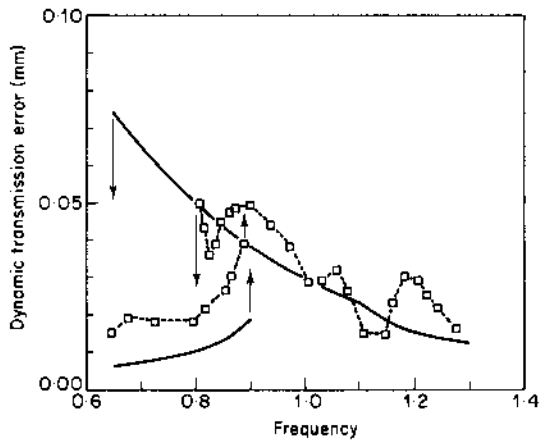

Figure 21. Comparison of theory with Munro's [13] experiments at 1/2 of design load. Key as Figure 19.

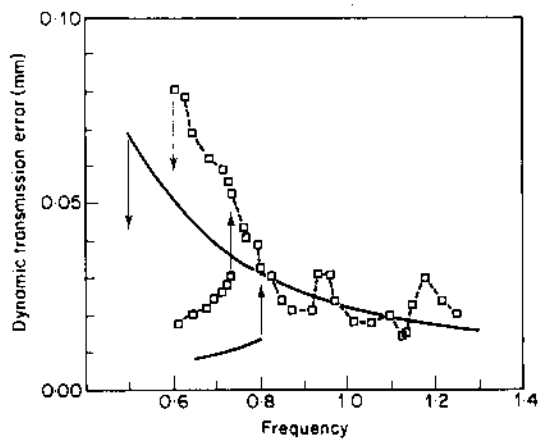

Figure 22. Comparison of theory with Munro's [13] experiments at 1/4 of design load. Key as Figure 19.

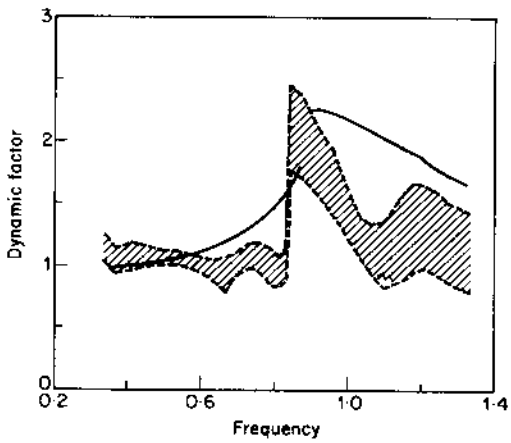

Figure 23. Comparison of theory (——) with experimental results of Kubo (– – –) (extracted from reference [9]).

reasons for the discrepancy including the usage of D_L instead of D_S, the validity of the computer model used to calculate $\bar{e}(\bar{t})$, insufficient knowledge of some system parameters such as profile modifications, and the assumptions made in developing our theory, such as the time invariant mesh stiffness. Therefore the experimental data is not exactly analogous to our analytical predictions even though a satisfactory agreement is found. Obviously our theory should be refined in order to obtain a better agreement with Kubo's data; for instance, time-varying mesh stiffness may be included.

8. COMPARISON OF EXCITATIONS

8.1. INTERNAL VERSUS EXTERNAL EXCITATION

First, we assume that only one type of excitation exists at a time and compare the frequency response characteristics of the system due to the internal static transmission error sinusoidal excitation $F_i(t)$ given by equation (5) with the external sinusoidal excitation $F_e(t)$ given by equation (4). The comparison is based on the analytical solutions which are constructed in section 4 for equation (5) and in reference [20] for equation (4). In the case of internal excitation, the amplitude of the alternating force has a Ω_h^2 term which makes the alternating force amplitude frequency dependent. This amplitude $F_{ah}\Omega_h^2$ is smaller than F_{ah} for $\Omega_h < 1$ and greater than F_{ah} when $\Omega_h > 1$. Hence the overall alternating force amplitude ratio $F_m/F_{ah}\Omega_h^2$ varies with Ω_h even though $\hat{F} = F_m/F_{ah}$ is kept constant. In the case of external excitation, the force amplitude ratio $\hat{F} = F_m/F_{aT}$ is frequency independent.

The frequency responses for four values of $\hat{F}$ given $F_m = 0{\cdot}1$, $\Omega_h = \Omega_T = \Omega$ and $\zeta = 0{\cdot}05$ are compared in Figures 24 and 25. When $\hat{F}$ is sufficiently large, say $\hat{F} \geqslant 10$, only case I solutions corresponding to the no-impact (case I) exist. Accordingly, both excitations result in the linear system responses which are close to each other for $\Omega < 1$; but for $\Omega > 1$ there is a difference which grows with increasing frequency Ω as shown in Figure 24(a). When $\hat{F}$ is reduced to 2, both case I and case II regimes exist; the difference between two excitations is again significant at higher Ω as shown in Figure 24(b). The transition frequencies also differ, and a larger range of dual-valued solutions is seen for equation (5). Case III solutions are witnessed at lower values of $\hat{F}$ (1 and 0·5) as shown in Figures 25(a) and 25(b). While equation (5) always has a case I regime at low Ω, equation (4) does not produce case I at $\hat{F} = 0{\cdot}5$. Another important observation from

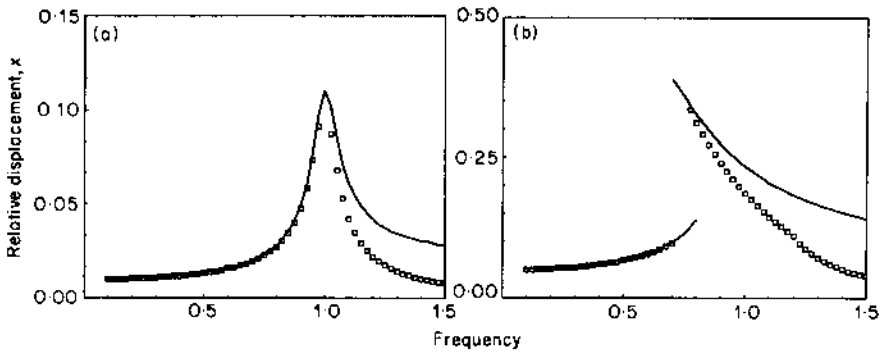

Figure 24. Comparison of the frequency response due to the external torque excitation (□) given by Comparin and Singh [20] and the static transmission error excitation (——); $\zeta = 0{\cdot}05$, $F_m = 0{\cdot}1$, $\Omega_h = \Omega_T$ and (a) $\hat{F} = 10$, (b) $\hat{F} = 2$.

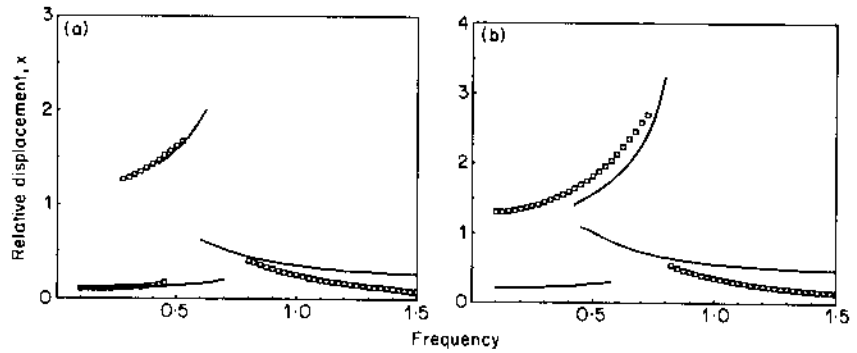

Figure 25. Comparison of the frequency response due to the external torque excitation (□) given by Comparin and Singh [20] and the static transmission error excitation (——); $\zeta = 0{\cdot}05$, $F_m = 0{\cdot}1$, $\Omega_h = \Omega_T$ and (a) $\hat{F} = 1$, (b) $\hat{F} = 0{\cdot}5$.

Figures 24 and 25 is that up to two steady state solutions are seen in the external torque excitation case; conversely as many as three soutions are found for the geared system excited by the static transmission error.

8.2. PERIODIC OR COMBINED EXCITATION

The approximate analytical solutions given in section 4 are constructed only for a single harmonic internal excitation term $\bar{e}(\bar{t})$ or $F_i(t)$. However, in the real geared systems, $\bar{e}(\bar{t})$ or $F_i(t)$ is periodic and can be represented by a Fourier series of fundamental frequency Ω_h. Therefore, it is necessary to consider the higher harmonics of $F_i(t)$ besides the fundamental component which is already included in the analysis. On the other hand, both external $F_e(t)$ and internal $F_i(t)$ excitations may exist simultaneously. These two cases require that $F(t)$ in equation (3) be reformulated as follows:

$$F(t) = F_m + F_e(t) + F_i(t)$$

$$= F_m + \sum_{j=1}^{k} F_{aTj} \sin(j\Omega_T t + \phi_{Tj}) + \sum_{j=1}^{k} (j\Omega_h)^2 F_{ahj} \sin(j\Omega_h t + \phi_{hj}). \tag{20}$$

In order to construct analytical solutions for this $F(t)$, we must investigate the applicability of the principle of superposition: i.e., of considering first each excitation separately and then superposing the corresponding responses to generate the overall frequency

response. Two cases are considered and the analytical results based on the principle of superposition are verified through digital simulation.

Consider only the static transmission error excitation $F_i(t)$ in equation (20) with three harmonics: i.e.,

$$F_e(t) \quad \text{and} \quad F(t) = F_m + \sum_{j=1}^{3} (j\Omega_h)^2 F_{ahj} \sin(j\Omega_h t + \phi_{hj}).$$

The amplitudes of the harmonics are selected to be $F_{ah1} = 0{\cdot}05$, $F_{ah2} = 0{\cdot}02$ and $F_{ah3} = 0{\cdot}01$, and the mean force $F_m = 0{\cdot}1$. First each excitation component is considered separately without paying any attention to the phase angles and the frequency responses are obtained by using digital simulation; these are shown in Figure 26. Second, all three excitations are included simultaneously; this overall response is also shown in Figure 26, for comparison with the previous solutions. The frequency response due to each harmonic of the excitation is very close to the overall solution around the resonance peaks governed by that harmonic. When all of the solutions corresponding to each harmonic are added algebraically by considering the phase angles also, the overall response improves as shown in Figure 27. This response is in the form $q_a(t) = \sum_{j=1}^{3} q_{aj} \sin(j\Omega_h t + \phi_{hj})$, where q_{aj} is the alternating displacement when only the jth harmonic is considered. It is suggested in Figure 27 that the principle of superposition can be applied to a gear pair with backlash, provided that the excitation frequencies are sufficiently far apart from each other. In the case of periodic static transmission excitation, this is valid as all excitation frequencies are at least Ω_h apart.

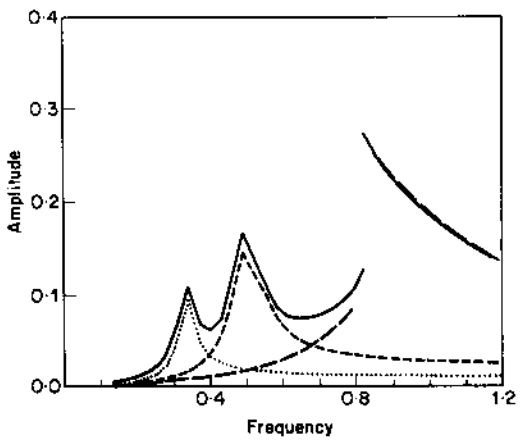

Figure 26. Comparison of the frequency response q_a due to first three harmonics of the static transmission error for the cases when the harmonics are considered simultaneously and separately; $F_m = 0{\cdot}1$, $\zeta = 0{\cdot}05$, $F_{ah1} = 0{\cdot}05$, $F_{ah2} = 0{\cdot}02$ and $F_{ah3} = 0{\cdot}01$. These results were obtained by using digital simulation. ——, First three harmonics simultaneously; — — —, 1st harmonic; - - - -, 2nd harmonic; . . . . . , 3rd harmonic.

Now, the principle of superposition, which has been already verified by digital simulation, can be used to obtain the approximate analytical solutions per section 4 when the periodic forcing function is considered. In Figure 28 is shown the analytical frequency response curve for $F_m = 0{\cdot}1$, $F_{ah1} = 0{\cdot}05$, $F_{ah2} = 0{\cdot}02$, $F_{ah3} = 0{\cdot}01$ and $\zeta = 0{\cdot}05$. Here the jump discontinuity is seen only at the peak Ω_{h1} governed by F_{ah1} since F_m/F_{ah2} and F_m/F_{ah3} are both sufficiently high so that no tooth separation occurs at Ω_{h2} and Ω_{h3}, respectively. However, the jump phenomenon can also be seen at the higher harmonics

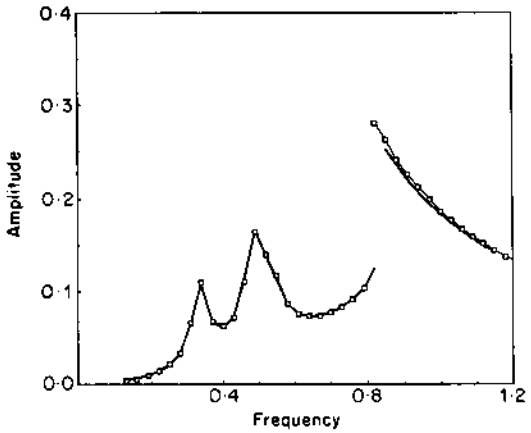

Figure 27. Comparison of digital simulation results obtained by using the principle of superposition (—□—) and by considering all three harmonic excitations applied simultaneously (——); $F_m = 0{\cdot}1$, $\zeta = 0{\cdot}05$, $F_{ah1} = 0{\cdot}05$, $F_{ah2} = 0{\cdot}02$ and $F_{ah3} = 0{\cdot}01$. In this case, phase angles are included in the superposition.

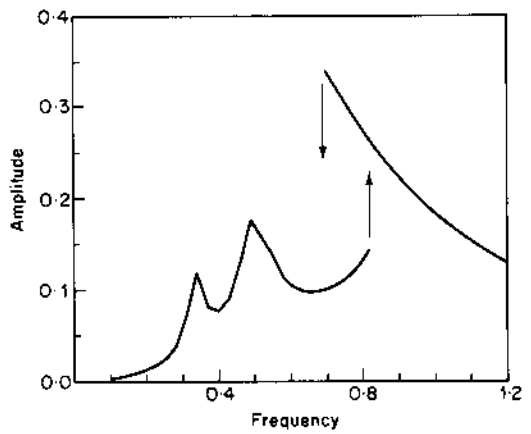

Figure 28. Comparison of the frequency response q_a due to the first three harmonics of the static transmission error. This curve is based on the principle of superposition applied to the analytical solutions which have been constructed by the method of harmonic balance; $F_m = 0{\cdot}1$, $\zeta = 0{\cdot}05$, $F_{ah1} = 0{\cdot}05$, $F_{ah2} = 0{\cdot}02$ and $F_{ah3} = 0{\cdot}01$.

depending on the force ratios F_m/F_{ahj}, $j \neq 1$ and ζ in accordance with the results of section 6. The same concept can be applied to the superharmonic components of the external torque excitation of equation (20) provided that $F_{ahj} = 0$.

The principle of superposition is now extended to the case where both internal $F_i(t)$ and external $F_e(t)$ sinusoidal excitations exist simultaneously as given by equation (3) provided that the excitation frequencies Ω_h and Ω_T are not close to each other. In a real geared system, Ω_h is much higher than Ω_T, which implies that the principle of superposition should be suitable for this case. In Figure 29 are illustrated the frequency response solutions due to the fundamental harmonic component of both excitations for $F_m = 0{\cdot}1$, $F_{ah1} = F_{aT1} = 0{\cdot}05$, $\zeta = 0{\cdot}05$ and by assuming that $\Omega_h = 2\Omega_T$. Here, the jump discontinuity is seen at two frequencies. However, when $\Omega_h \approx \Omega_T$ or when one of the superharmonic peaks of $F_i(t)$ coincides with the resonant peak governed by $F_e(t)$, the principle of

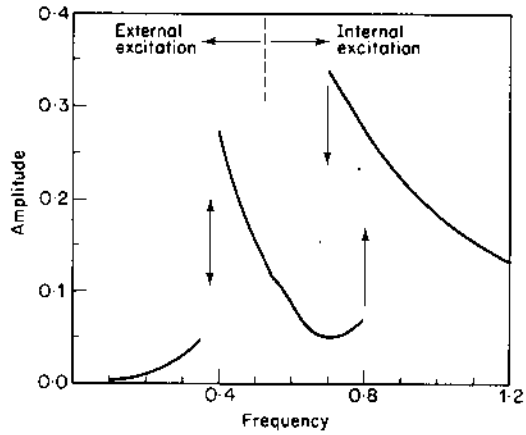

Figure 29. Frequency response q_a due to both the external torque and the static transmission error excitations. This curve is based on the principle of superposition applied to the analytical solutions which have been constructed by the method of harmonic balance; $F_m = 0{\cdot}1$, $\zeta = 0{\cdot}05$, $F_{ah} = 0{\cdot}05$, $F_{aT} = 0{\cdot}05$, $\Omega_h = 2\Omega_T$.

superposition will no longer be applicable. In such cases, we will use the digital simulation as the analytical interpretation of these cases is yet to be explored.

9. CONCLUSION

This analytical study of the non-linear dynamics of a spur gear pair with backlash as excited by the static transmission error has made a number of contributions to the state of the art. First, difficulties associated with the digital simulation technique have been resolved as multiple steady state solutions at a given frequency can be found provided that the entire initial condition map is searched. Second, new frequency response solutions for the gear pair have been constructed by using the method of harmonic balance. Third, our mathematical models have been validated as these compare well with results of two previous experimental studies and the key parameters such as the mean load, mean to alternating force ratio, damping and backlash have been identified. Fourth, the chaotic and subharmonic resonances are observed if the mean load is too small for a lightly damped system. Fifth, mathematical conditions for tooth separation and back collision have been established which are compatible with available measured data. Sixth, the periodic transmission error excitation case has been analyzed by using the method of harmonic balance in conjunction with the principle of superposition. Finally, on a more fundamental note, our study enriches the current literature on the clearance non-linearity or vibro-impact systems as the governing non-linear differential equation is different from the conventional single-degree-of-freedom system formulation.

Our ongoing research work is focused on the inclusion of the following in our proposed formulations: geared drive prime mover and load inertias, shaft and bearing compliances, bearing non-linearities including clearances and preload or preset problems, time-varying mesh stiffness and interactions between bearing non-linearities and backlash. Also, efforts are under way to conduct frequency response measurements on an experimental test facility which will be used to verify or refine our theory further. In future, we intend to examine single and multi-mesh non-linear dynamic problems in other types of geared drives.

ACKNOWLEDGMENTS

We thank NASA Lewis Research Center for supporting this study and D. R. Houser for his guidance.

REFERENCES

1. D. DUDLEY 1984 *Handbook of Practical Gear Design.* New York: McGraw-Hill.
2. D. B. WELBOURN 1979 *Proceedings of the Conference on Noise and Vibrations of Engines and Transmissions, Institution of Mechanical Engineers,* 9–14. Fundamental knowledge of gear noise—a survey.
3. D. R. HOUSER 1988 *Proceedings of Inter-Noise* 88. 601–606. Gear noise state of the art.
4. C. TROEDER, H. PEEKEN, A. LASCHET and K. TOOTEN 1983 *Proceedings of International Federation of the Theory of Machines and Mechanisms Sixth World Congress, New Delhi* **2**, 936–943. Causes and effect of torque change in hammering of toothed gears.
5. T. HAYASHI, N. NISHI, T. OHNO and F. R. E. CROSSLEY 1979 *Proceedings of the Fourth World Congress on the Theory of Machines and Mechanisms,* 350–353. Multiple impacts of a cylinder between two planes and of a meshing teeth of a pair of gears.
6. M. S. TAVAKOLI and D. R. HOUSER 1986 *Journal of Mechanisms, Transmissions and Automation in Design, Transactions of the Amerian Society of Mechanical Engineers* **108**, 86–95. Optimum profile modifications for the minimization of static transmission errors of spur gears.
7. R. G. MUNRO 1967 *The Aerospace Committeee Meeting of the Amerian Gear Manufacturers Association,* 1–11. Gear transmission error.
8. W. D. MARK 1987 *Journal of Mechanisms, Transmissions and Automation in Design, Transactions of the American Society of Mechanical Engineers* **109**, 283–291. Use of the generalized transmission error in the equations of motion of gear systems.
9. H. N. OZGUVEN and D. R. HOUSER 1988 *Journal of Sound and Vibration* **125**, 71–83. Dynamic analysis of high speed gears by using loaded static transmission error.
10. K. ICHIMARU and F. HIRANO 1974 *Journal of Engineering for Industry, Transactions of the American Society of Mechanical Engineers* **96**, 373–381. Dynamic behavior of heavily-loaded spur gears.
11. E. P. REMMERS 1971 *American Society of Mechanical Engineers Paper* 71-DE-23. The dynamics of a gear pair system.
12. A. KAHRAMAN, H. N. OZGUVEN, D. R. HOUSER and J. ZAKARAJSEK 1989 *Proceedings of Fifth International Power Transmission and Gearing Conference, American Society of Mechanical Engineers,* 375–382. Dynamic analysis of geared rotors by finite elements.
13. R. G. MUNRO 1962 *Ph. D. Dissertation, Cambridge University.* The dynamic behaviour of spur gears.
14. A. KUBO, K. YAMADA, T. AIDA and S. SATO 1972 *Transactions of the Japan Society of Mechanical Engineers* **38**, 2692–2715. Research on ultra high speed gear devices (reports 1–3).
15. K. UMEZAWA, T. SATA and J. ISHIKAWA 1984 *Bulletin of the Japan Society of Mechanical Engineers* **38**, 102–109. Simulation of rotational vibration of spur gears.
16. H. N. OZGUVEN and D. R. HOUSER 1988 *Journal of Sound and Vibration* **121**, 383–411. Mathematical models used in gear dynamics—a review.
17. T. SAKAI, Y. DOI, K. YAMATOMO, T. OGASAWARA and M. NARITA 1981 *SAE Paper* 810773. Theoretical and experimental analysis of rattling noise of automotive gearbox.
18. S. OHNUMA, Y. SHIGETARO, I. MINEICHI and T. FUJIMOTO 1985 *SAE Paper* 850979. Research on the idling rattle of manual transmission.
19. D. C. H. YANG and J. Y. LIN 1987 *Journal of Mechanisms, Transmissions and Automation in Design, Transactions of the American Society of Mechanical Engineers* **109**, 189–196. Hertzian damping, tooth friction and bending elasticity in gear impact dynamics.
20. R. J. COMPARIN and R. SINGH 1989 *Journal of Sound and Vibration* **134**, 259–290. Nonlinear frequency response characteristics of an impact pair.
21. R. SINGH, H. XIE and R. J. COMPARIN 1989 *Journal of Sound and Vibration* **131**, 177–196. Analysis of an automotive neutral gear rattle.
22. F. KUCUKAY 1984 *Proceedings of the Third Conference on Vibrations of Rotating Machinery, Institution of Mechanical Engineers,* 73–79. Dynamic loads in gear teeth.
23. R. C. AZAR and F. R. E. CROSSLEY 1977 *Journal of Engineering for Industry, Transactions of the American Society of Mechanical Engineers* **99**, 792–798. Digital simulation of impact phenomenon in spur gear systems.

24. K. NAKAMURA 1967 *Bulletin of The Japan Society of Mechanical Engineers* **10**, 846–854. Tooth separation and abnormal noise on power transmission gears.
25. H. H. LIN, R. L. HUSTON and J. J. COY 1987 *NASA Technical Memorandum* 100180. On dynamic loads in parallel shaft transmissions, I-modeling and analysis.
26. C. W. GEAR 1984 *Computer Aided Analysis and Optimization of Mechanical Systems, NATO ASI Series* **F9**, 323–334. Differential-algebraic equations.
27. C. W. GEAR 1984 *Computer Aided Analysis and Optimization of Mechanical Systems, NATO ASI Series* **F9**, 335–349. The numerical solution of problems which may have high frequency components.
28. C. C. WANG 1978 *Journal of Mechanical Design, Transactions of the American Society of Mechanical Engineers* **100**, 363–373. Rotational vibration with backlash: Part 1.
29. C. C. WANG 1981 *Journal of Mechanical Design, Transactions of the American Society of Mechanical Engineers* **103**, 387–397. Rotational vibration with backlash: Part 2.
30. S. W. SHAW and P. J. HOLMES 1983 *Journal of Sound and Vibration* **90**, 129–155. A periodically forced piecewise linear oscillator.
31. F. C. MOON and S. W. SHAW 1983 *International Journal of Non-Linear Mechanics* **18**, 465–477. Chaotic vibrations of a beam with non-linear boundary conditions.
32. G. S. WHISTON 1979 *Journal of Sound and Vibration* **67**, 179–186. Impacting under harmonic excitation.
33. G. S. WHISTON 1987 *Journal of Sound and Vibration* **115**, 303–319. The vibro-impact response of a harmonically excited and preloaded one-dimensional linear oscillator.
34. G. S. WHISTON 1987 *Journal of Sound and Vibration* **118**, 395–429. Global dynamics of a vibro-impacting linear oscillator.
35. Y. UEDA 1980 *New Approaches to Nonlinear Problems in Dynamics*, 311–322. Steady motions exhibited by Duffing's equation: a picture book of regular and chaotic motion. Philadelphia: SIAM.
36. J. M. T. THOMPSON and H. B. STEWART 1986 *Nonlinear Dynamics and Chaos*. Chichester: John Wiley
37. IMSL INC. 1986 *IMSL Users Manual*.
38. A. GELB and W. E. VAN DER VELDE 1968 *Multiple Input Describing Functions and Nonlinear System Design*. New York: McGraw-Hill.

APPENDIX: LIST OF SYMBOLS

b	backlash
c	viscous damping coefficient
d	diameter
e	static transmission error
f	non-linear displacement function
F	force
g, h	non-linear functions
I	rotary inertia
k	stiffness
m	mass
N, N^*	describing functions
q	displacement
t	time
T	torque
x	dynamic transmission error
ϕ	phase angle
φ	an angle
θ	rotational displacement
σ	stress
ω_n	resonant frequency
Ω	excitation frequency
ζ	damping ratio

Subscripts

a	alternating component
c_1, c_2	reference quantities
d	dynamic
e	external
$g1$	pinion
$g2$	gear
h	gear mesh
i	internal
L	load
m	mean component
p	period
r	response
s	static
S	stress
T	torque
I, II, III	case index

Superscripts

$\bar{}$	dimensional quantities†
$\tilde{}$	amplitude of a harmonic function
$\dot{}$	derivative with respect to time
$\hat{}$	force ratio

† All dimensionless quantities are shown without any superscript